Supplementary Materials

N, O co-doped hierarchically porous carbon derived from pitch/g-C_3N_4 composite for high-performance zinc-ion hybrid supercapacitors

Miaomiao Zhang[#], Ende Cao[#], Ruilun Xie[*], Guangming Rong, Tianyu Chen, Xiangchun Liu, Zhao Lei, Qiang Ling, Zhigang Zhao, Yujiao Tian[*]

School of Chemistry & Chemical Engineering, Anhui Province Key Laboratory of Coal Clean Conversion & High Valued Utilization, Anhui University of Technology, Ma'anshan 243032, Anhui, China.

[#]Authors contributed equally.

Correspondence to: Dr. Ruilun Xie, Dr. Yujiao Tian, School of Chemistry & Chemical Engineering, Anhui Province Key Laboratory of Coal Clean Conversion & High Valued Utilization, Anhui University of Technology, Ma'anshan 243002, Anhui, China. E-mail: Ruilunxie@126.com; tyjiao@163.com

Supplementary Table 1. Proximate and ultimate analyses of coal tar pitch

Proximate analysis (*wt*%)				Ultimate analysis (*wt*% daf)				
M_{ad}	A_d	V_{daf}	FC_{daf}^*	C	H	N	S	O^*
0.08	1.00	55.80	43.12	91.34	4.01	1.03	0.43	3.19

*: by difference.

Supplementary Table 2. N_2 adsorption-desorption isotherm parameters of M-C_3N_4-x samples

Sample	S_{BET} ($m^2 \cdot g^{-1}$)	$S_{t\text{-}Plot/micro}$ ($m^2 \cdot g^{-1}$)	$S_{BJH/meso}$ ($m^2 \cdot g^{-1}$)	V_{total} ($cm^3 \cdot g^{-1}$)	V_{micro} ($cm^3 \cdot g^{-1}$)
M-C_3N_4-0.5	666.28	120.82	379.89	0.41	0.06
M-C_3N_4-1	943.01	82.18	553.88	0.56	0.04
M-C_3N_4-2	1001.58	194.54	516.70	0.58	0.11

Supplementary Table 3. Content of C, N and O in M-C_3N_4-x samples

Atomic (*at*%)	C 1*s*	N 1*s*	O 1*s*
M-C_3N_4-0.5	87.37	3.72	8.91
M-C_3N_4-1	88.17	5.11	6.72
M-C_3N_4-2	87.14	6.32	6.54

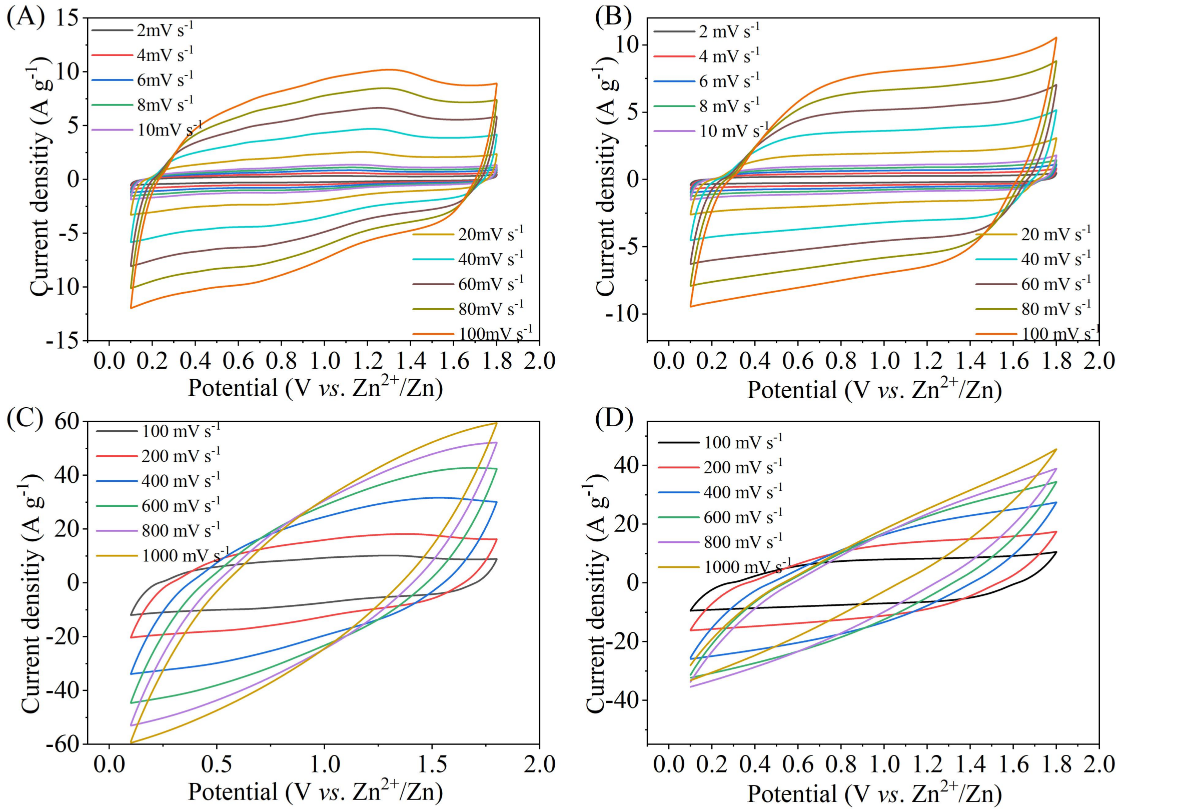

Supplementary Figure 1. (A) CV curves of M-C_3N_4-0.5//Zn ZIHSC and (B) M-C_3N_4-1//Zn ZIHSC at 2~100 mV·s^{-1}; (C) CV curves of M-C_3N_4-0.5//Zn ZIHSC and (D) M-C_3N_4-1//Zn ZIHSC at 100~1,000 mV·s^{-1}.

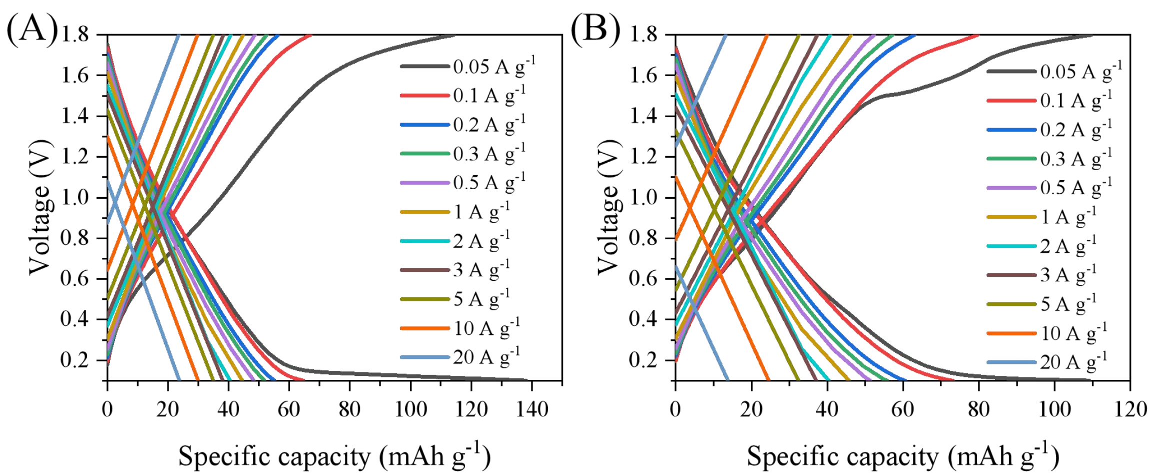

Supplementary Figure 2. GCD curves of (A) M-C_3N_4-1//Zn and (B) M-C_3N_4-0.5//Zn ZIHSCs.

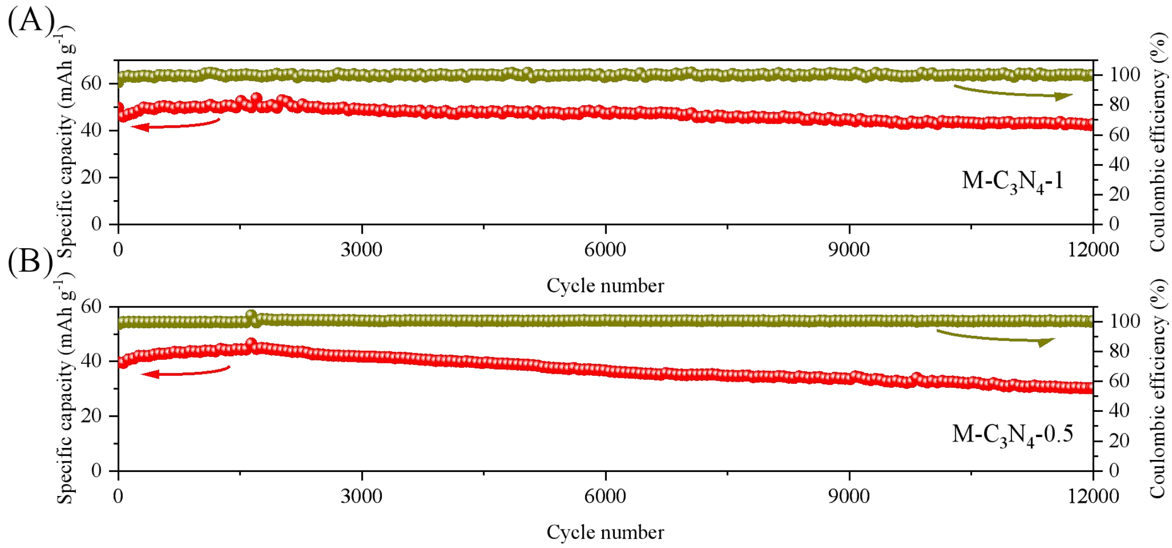

Supplementary Figure 3. GCD cycling stabilities of (A) $M\text{-}C_3N_4\text{-}1$//Zn and (B) $M\text{-}C_3N_4\text{-}0.5$//Zn ZIHSCs at 1 $A{\cdot}g^{-1}$.

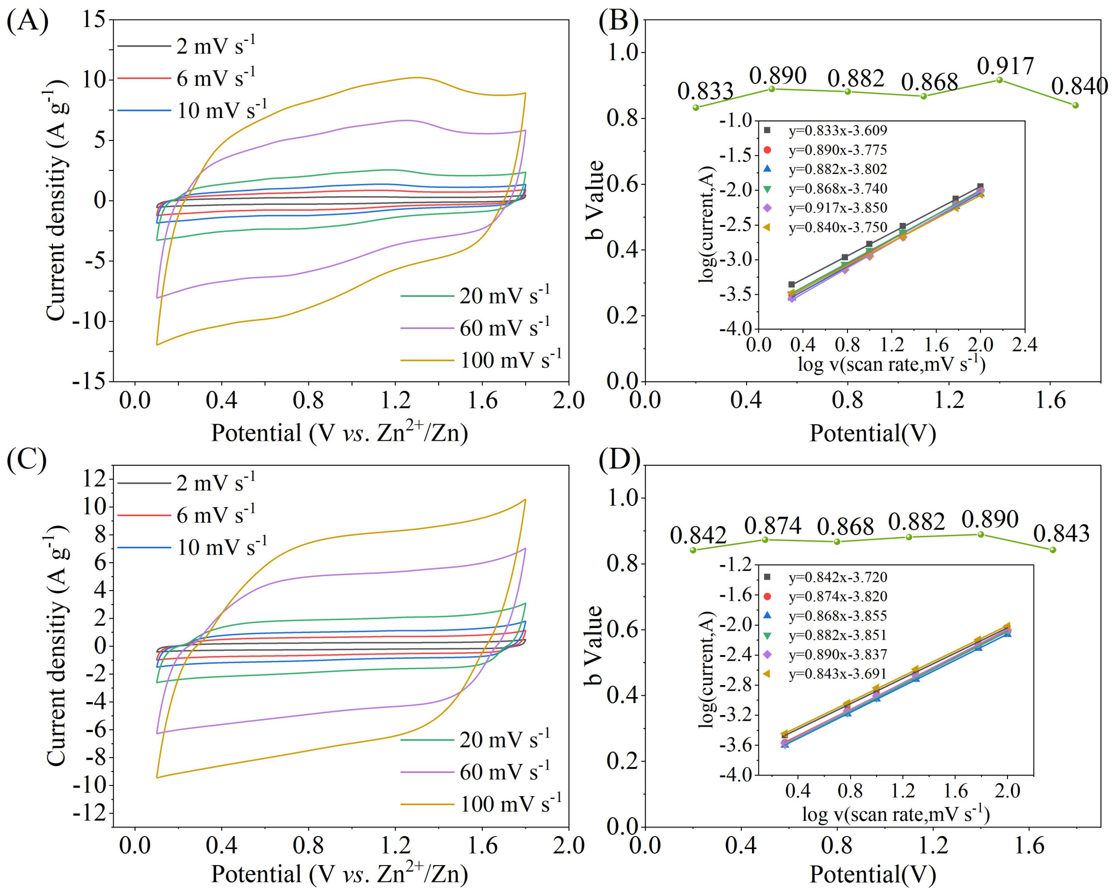

Supplementary Figure 4. (A) CV curves of $M\text{-}C_3N_4\text{-}0.5$//Zn ZIHSC at 2~100 $mV{\cdot}s^{-1}$; (B) *b* values of $M\text{-}C_3N_4\text{-}0.5$//Zn ZIHSC (the embedded graph is a linear fit curve); (C) CV curves of $M\text{-}C_3N_4\text{-}1$//Zn ZIHSC at 2~100 $mV{\cdot}s^{-1}$; (D) *b* values of $M\text{-}C_3N_4\text{-}1$//Zn ZIHSC (the embedded graph is a linear fit curve).

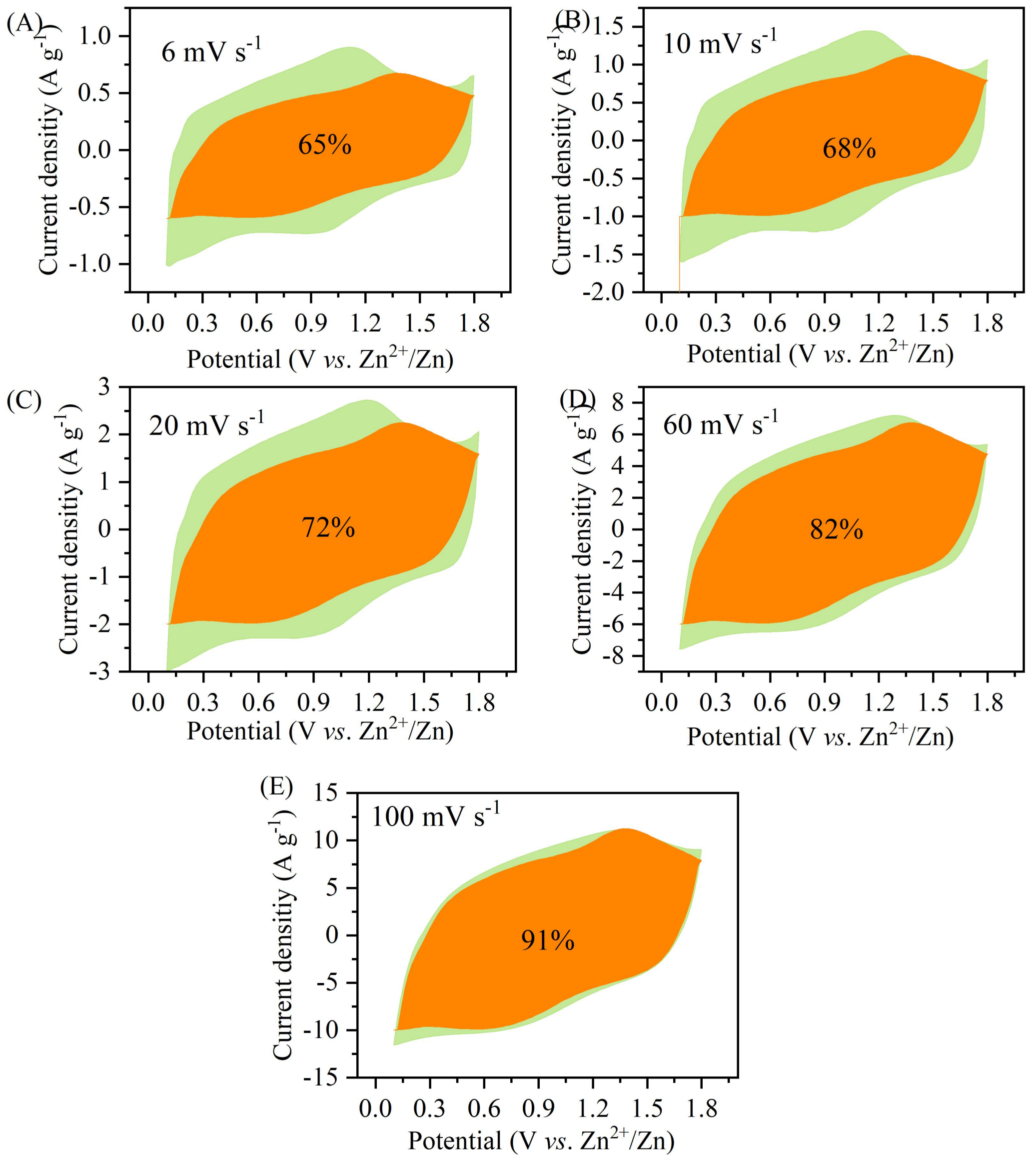

Supplementary Figure 5. Schematic representation of the capacitive contribution of M-C_3N_4-2//Zn ZIHSC at scanning rate of (A) 6 mV·s^{-1}; (B) 10 mV·s^{-1}; (C) 20 mV·s^{-1}; (D) 60 mV·s^{-1}; and (E) 100 mV·s^{-1}.

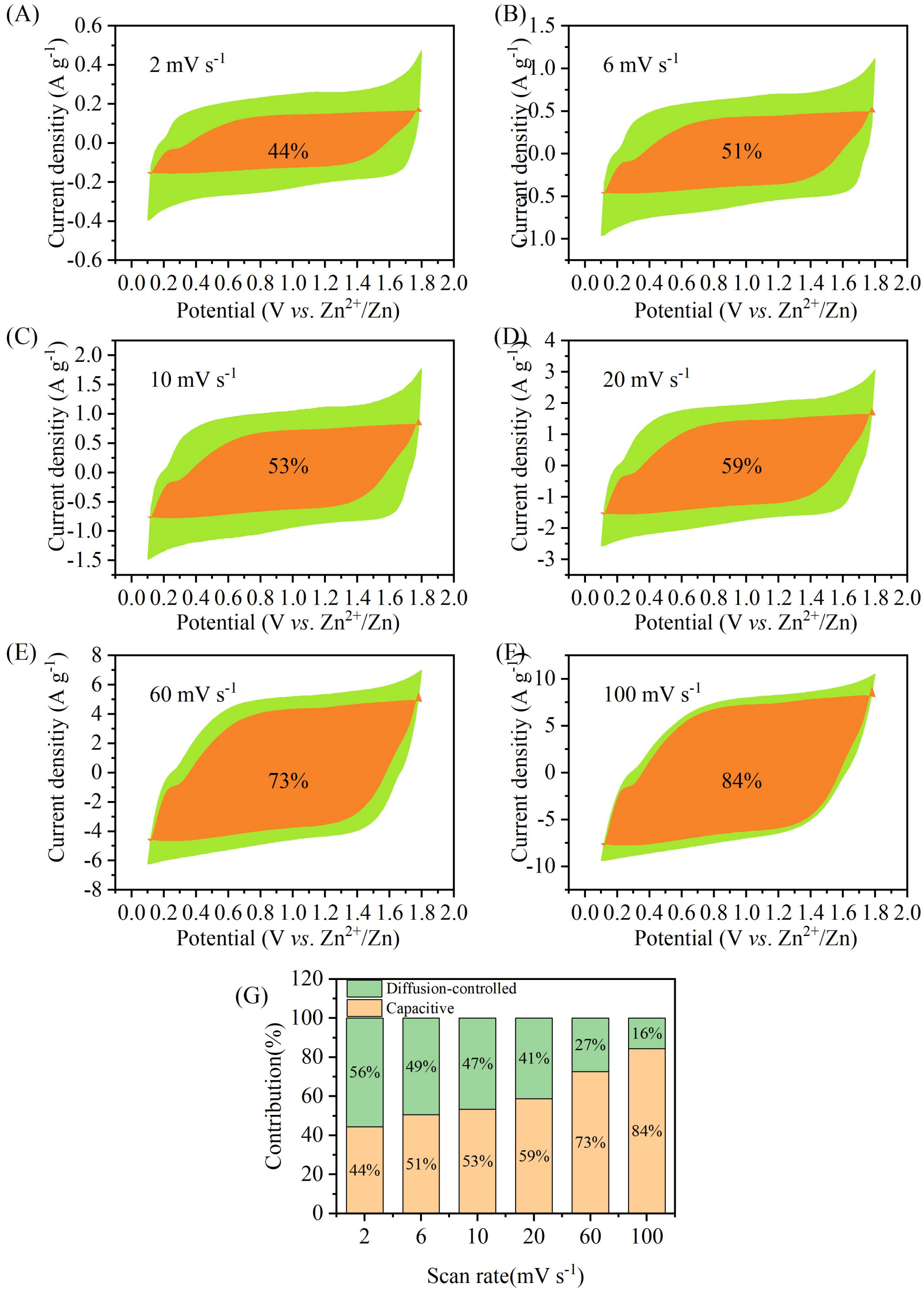

Supplementary Figure 6. Schematic representation of the capacitive contribution of M-C_3N_4-1//Zn ZIHSC at scanning rate of (A) 2mV·s^{-1}; (B) 6 mV·s^{-1}; (C) 10 mV·s^{-1}; (D) 20 mV·s^{-1}; (E) 60 mV·s^{-1}; and (F) 100 mV·s^{-1}; (G) Capacitance contribution of M-C_3N_4-1//Zn ZIHSC at 2~100 mV·s^{-1}.

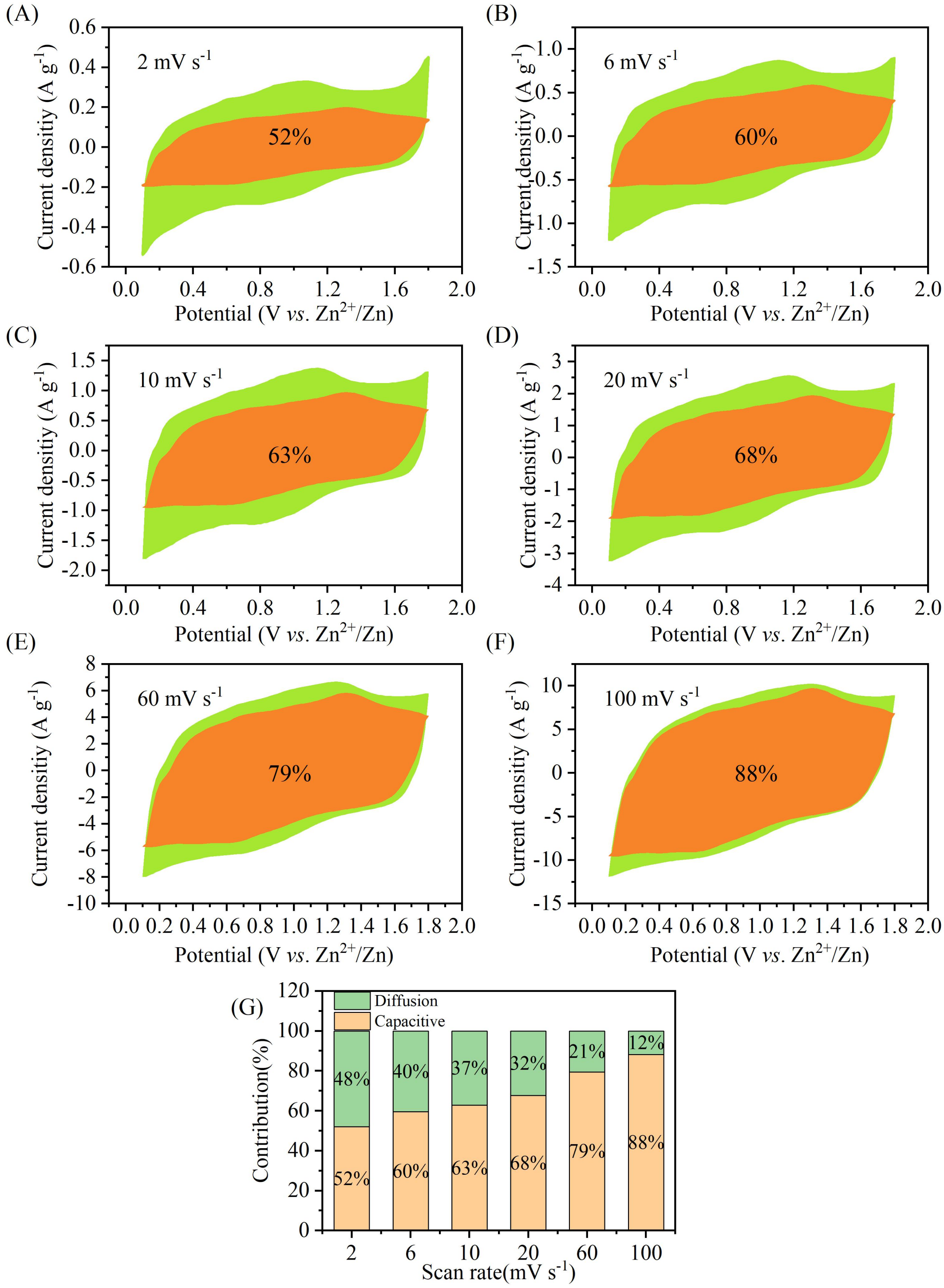

Supplementary Figure 7. Schematic representation of the capacitive contribution of M-C_3N_4-0.5//Zn ZIHSC at scanning rate of (A) 2mV·s^{-1}; (B) 6 mV·s^{-1}; (C) 10 mV·s^{-1}; (D) 20 mV·s^{-1}; (E) 60 mV·s^{-1}; and (F) 100 mV·s^{-1}; (G) Capacitance contribution of M-C_3N_4-0.5//Zn ZIHSC at 2~100 mV·s^{-1}.